

PHYSICS CONTRIBUTION

BIOLOGICAL *IN SITU* DOSE PAINTING FOR IMAGE-GUIDED RADIATION THERAPY USING DRUG-LOADED IMPLANTABLE DEVICES

ROBERT A. CORMACK, PH.D.,* SRINIVAS SRIDHAR, PH.D.,[†] W. WARREN SUH, M.D., M.P.H.,*
ANTHONY V. D'AMICO, M.D., PH.D.,* AND G. MIKE MAKRIGIORGOS, PH.D.*

*Department of Radiation Oncology, Dana Farber Cancer Institute, Brigham and Women's Hospital, Harvard Medical School, Boston, Massachusetts; and [†]Electronics Materials Research Institute, Northeastern University, and Department of Physics, Northeastern University, Boston, Massachusetts

Purpose: Implantable devices routinely used for increasing spatial accuracy in modern image-guided radiation treatments (IGRT), such as fiducials or brachytherapy spacers, encompass the potential for *in situ* release of biologically active drugs, providing an opportunity to enhance the therapeutic ratio. We model this new approach for two types of treatment.

Methods and Materials: Radiopaque fiducials used in IGRT, or prostate brachytherapy spacers ("eluters"), were assumed to be loaded with radiosensitizer for *in situ* drug slow release. An analytic function describing the concentration of radiosensitizer versus distance from eluters, depending on diffusion–elimination properties of the drug in tissue, was developed. Tumor coverage by the drug was modeled for tumors typical of lung stereotactic body radiation therapy treatments for various eluter dimensions and drug properties. Six prostate ¹²⁵I brachytherapy cases were analyzed by assuming implantation of drug-loaded spacers. Radiosensitizer-induced subvolume boost was simulated from which biologically effective doses for typical radiosensitizers were calculated in one example. **Results:** Drug distributions from three-dimensional arrangements of drug eluters versus eluter size and drug properties were tabulated. Four radiosensitizer-loaded fiducials provide adequate radiosensitization for ~4-cm-diameter lung tumors, thus potentially boosting biologically equivalent doses in centrally located stereotactic body treated lesions. Similarly, multiple drug-loaded spacers provide prostate brachytherapy with flexible shaping of "biologically equivalent doses" to fit requirements difficult to meet by using radiation alone, e.g., boosting a high-risk region juxtaposed to the urethra while respecting normal tissue tolerance of both the urethra and the rectum.

Conclusions: Drug loading of implantable devices routinely used in IGRT provides new opportunities for therapy modulation via biological *in situ* dose painting. © 2010 Elsevier Inc.

Image-guided radiation therapy, Fiducials, Brachytherapy seeds, Lung SBRT treatment.

INTRODUCTION

Despite advances in the precision, accuracy, and mode of therapy delivery, the effective use of present day radiation therapy modalities (intensity-modulated radiation therapy, image-guided radiation therapy [IGRT], brachytherapy, protons) remains limited by the radiation dose to normal structures surrounding the target region. Image-guided lung stereotactic body treatment achieves over 90% rates of tumor control for early-stage peripheral lesions. However, treatment of centrally located lung lesions to full dose (20 × 3 Gy) is associated with unacceptable toxicities (1), thus excluding a substantial fraction of patients from the benefits of new technology. Prostate cancer is another example where image-guided brachytherapy has made substantial progress (2, 3) but remains limited by normal tissue tolerance of adjacent

and interposed structures. The means to augment the biological action of radiation therapy in tumors without additional toxicity to surrounding normal tissues would be useful for improving the therapeutic ratio.

In order to achieve high spatial accuracy, modern radiation therapy practice routinely utilizes implantation of fiducials (external beam therapy) or source spacers (brachytherapy) into the tumor (4). These implantable devices are an essential technical component of the delivery of radiation but are inert and provide no direct therapeutic function. We propose that the routine introduction of these implantable devices in tumors provides opportunities for delivering *in situ* therapy or radiosensitization during IGRT as part of the established routine procedures. For example, coating radiopaque fiducials with polymers allowing slow release of radiosensitizers

Reprint requests to: G. Mike Makrigiorgos, Ph.D., Division of Medical Physics and Biophysics, Department of Radiation Oncology, DFCI-BWH Hospitals, 75 Francis Street, Boston, MA 02115. Tel: (617) 525-7122; Fax: (617) 582-6037; E-mail: mmakrigiorgos@lroc.harvard.edu

Conflict of interest: none.

Acknowledgment—This work was funded by a Kayes Scholars grant award.

Received Feb 17, 2009, and in revised form April 26, 2009. Accepted for publication June 4, 2009.

or cytotoxic compounds would allow fiducials to act as dual-functioning devices, providing both image guidance and *in situ* bioactive drug release. Such coatings have been described on titanium and aluminum (5) surfaces and on stents used in cardiology practice (6, 7). Similarly, spacers used to separate ^{125}I sources in prostate brachytherapy procedures can be replaced by polymeric rods (8, 9) acting as both spacers and drug-release molecules to provide additional flexibility in shaping biological dose distributions that avoid normal structures while boosting dose to the target. Since implantation of these devices is already part of current radiation therapy practice, use of drug-loaded fiducials and spacers would not cause any added risk or discomfort to patients during the implantation procedure.

We present a modeling study of drug distributions that would result from dual-action fiducials or dual-action brachytherapy spacers, assuming these are implanted in geometries commonly used during lung or prostate radiation treatments. We provide phenomenological modeling of drug concentration vs. effective diffusion distance that is independent of a particular choice of drug or tumor tissue type. The generalized approach describes the required balance between drug diffusion, elimination, and eluter size in order to achieve a desired drug distribution in the target volume. As we do not focus on a specific drug or radiosensitizer, agent-specific biological aspects of drug radiation interaction are not explicitly accounted for in this investigation. Instead, by assuming typical radiosensitization enhancements encountered in radiation oncology practice, we compare the ability to deliver a local increase in effective dose by either brachytherapy alone or by brachytherapy plus *in situ*-delivered radiosensitizer. Assisting IGRT treatment via the proposed biological *in situ* IGRT (BIS-IGRT) dose painting can be generalized beyond radiosensitizers to utilize a variety of molecularly targeted biological agents and to provide a practical means to translate recent developments in biological targeting agents to clinical radiation oncology practice.

METHODS AND MATERIALS

Analytic function for modeling drug diffusion from a chemical source

The concentration of drug versus the distance from a drug-eluting source can be modeled by the diffusion equation (10). Assuming a uniform diffusing medium around a spherical eluter, the diffusion equation may be expressed in spherical coordinates as

$$\frac{\partial A}{\partial t} = D \frac{1}{r^2} \frac{\partial}{\partial r} \left(r^2 \frac{\partial A}{\partial r} \right) \quad (1)$$

where r is radius, t represents time, A is drug concentration, and D is the diffusion constant. To model the distribution of drug around a drug-eluting object in tissue, accounting also for drug removal, Eq. 1 can be modified to include a term representing elimination of the drug:

$$\frac{\partial A}{\partial t} = D \frac{1}{r^2} \frac{\partial}{\partial r} \left(r^2 \frac{\partial A}{\partial r} \right) - kA \quad (2)$$

where k is a measure of the rate of elimination of the agent from the system by any means. For a first approximation, we have assumed

constant rates of drug release from the eluter and drug elimination in tissue. Under these conditions, it can be shown that a time-independent function that satisfies Eq. 2 is

$$A = \frac{A_0 a}{r} \exp(-\phi_b(r-a)) \quad (3)$$

where a is the radius of the eluter, $\phi_b = (k/D)^{1/2}$ is the elimination-diffusion modulus, and $r > a$. The parameter ϕ_b depends on the properties of the drug and medium chosen. Figure 1 illustrates a plot of Eq. 3 as a function of the distance from the center of a drug eluter, for two values of eluter radius and two values of ϕ_b . A lower value of ϕ_b increases the depth of penetration of the drug. Lower values of ϕ_b can be achieved either by increasing the diffusion length (D) or by decreasing the elimination constant (k). To provide a rough comparison with the attenuation of radiation with distance from a point radioactive source, the inverse square curve is also plotted. Values of the diffusion-elimination modulus ϕ_b plotted in Fig. 1 encompass the range of ϕ_b values (0.4–1.3 mm^{-1}), inferred from experimentally measured distribution of taxol as a function of distance from the eluter surface in the monkey brain (11, 12).

The diffusion distance of a drug in tissue can be modified in various ways, including adding of micelles (13) to change local hydrophilicity or lipophilicity or by using dextrans to increase convection. We (5) and others (14) have also shown that the drug can be loaded on nanoparticles which are then incorporated in the eluter. This approach does not change the chemical properties of the drug but takes advantage of the nanoparticle properties to change the effective rate of elimination and thus ϕ_b . Transport of nanoparticles and biomolecules in tumors is determined by the enhanced permeability and retention effect (15). The enhanced permeability facilitates drug delivery, while the retention, prolonged for weeks or months, can be therapeutically beneficial (15). Data for real-time tracking of quantum dot complexes of nanometer size in tumors (16) show that nanoparticle extravasation in the bloodstream displays both fast and slow movement, with speeds ranging from 100 to 600 $\mu\text{m/s}$. Large nanostructures such as liposomes, with diameters of 100 to 400 nm, appear to have even lower mobility (17). In summary, given multiple means to adjust the tissue diffusion properties of the drug, in this work ϕ_b and eluter radius are assumed to be parameters that can be modulated, and thus they are treated as variables.

Few eluters: fiducial markers

Commercially available cylindrical markers used in image-guided lung stereotactic body radiation therapy (SBRT) range from 0.8 to 1.2 mm in diameter and from 3 to 20 mm in length. However, for simplicity throughout this work, we simulated spherical eluters and used the radially symmetrical Eq. 3. To represent the range of fiducial sizes, we simulated small and large eluters (radii of 0.5 and 2 mm, respectively). We modeled four drug-loaded markers within a spherically shaped tumor with the eluters located at the vertices of a tetrahedron centered in the tumor, with the vertices being 5 mm from the tumor surface. The drug distribution is the sum of the distributions from each eluter, and the magnitude of the distribution is determined by A_0 , the drug concentration at the surface of the eluter. The distance at which the drug concentration drops by a factor of 10 is often used as a measure of effective tissue penetration by the drug (12, 13). Accordingly, the volume of tumor with a drug concentration in excess of $A_0/10$ is taken as the metric to quantify the fraction of tumor that is sensitized by the drug. The sensitized fraction of tumor volume (I) is calculated for multiple values of ϕ_b and eluter radius.

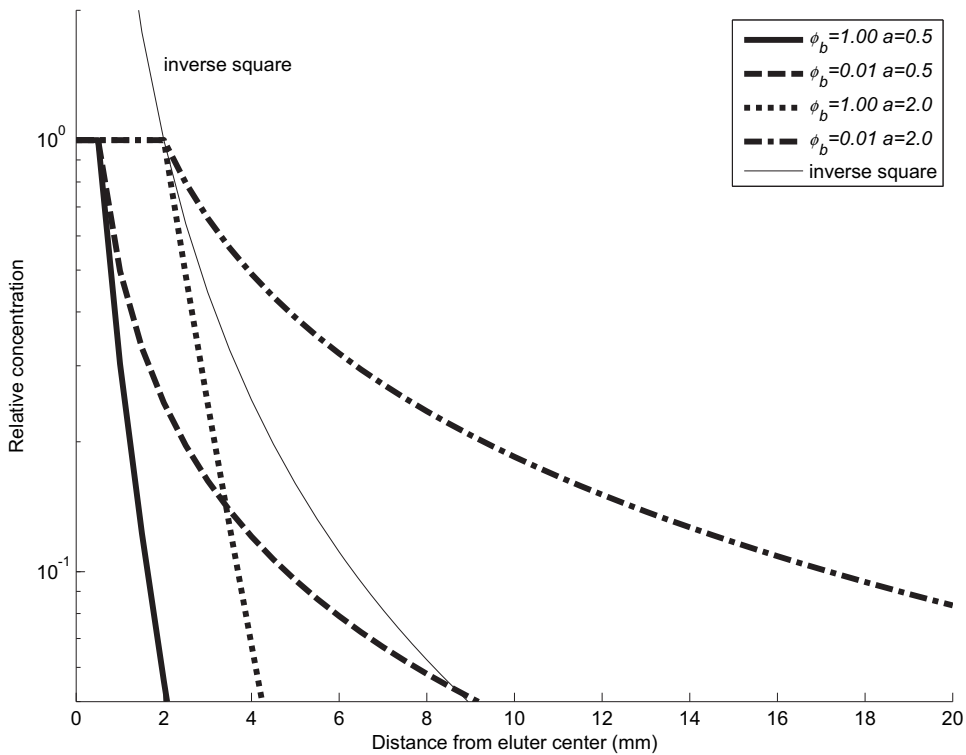


Fig. 1. Plots of Eq. 3 are shown for two source radii within a range of values of the elimination–diffusion modulus, ϕ_b . The chemical concentration is assumed to be 1 at the surface of the source. Larger source radii and smaller values of ϕ_b translate into greater effective penetration of the chemical agent into tissue. A plot of r^{-2} is shown for comparison with the dose distribution around a point radioactive source.

Several eluters: brachytherapy spacers

We use prostate brachytherapy as an example of a minimally invasive procedure that would utilize a large number of implanted eluters. It was assumed that the brachytherapy spacers used in ^{125}I transrectal ultrasound (TRUS)-guided permanent implants are replaced by drug eluters that also act as spacers. Brachytherapy treatment plans from 6 patients receiving permanent implants were reanalyzed to calculate chemical distributions that could be achieved without modifying the position of ^{125}I -sources and spacers used for delivery of the radiation treatment. Patients were selected to represent the range of gland sizes seen in our implant program. The location of eluting spacers was derived from the needle tip locations, as shown in Fig. 2. Thus, the location of the source at the tip of each needle was used to calculate all potential spacer locations. This does not imply that such spacers were actually in the plan but provides a set of potential spacer locations available without modification of the plan.

To evaluate the potential for a configuration of drug-loaded spacers to provide target coverage while sparing normal structures two quantities were evaluated, I_p , and G_{pr} , and the dependence of these metrics on ϕ_b was studied.

I_p
The coverage of the prostate $I_p(a)$ ($0 < a < 1$) is taken to be the fraction of prostate having a drug concentration greater than a . As described above, this work uses a value of $a = A_0/10$.

G_{pr}
For any line, L , specified by $x = x_o, z = y_o$, passing through prostate and rectum, the prostate–rectum gradient, $G(L)$, of a drug or radiation dose distribution $D(x,y,z)$ is given by $G(x_o,y_r,z_o) = D(x_o,y_r,z_o)/$

$D(x_o,y_p,z_o)$, where y_r is the most anterior point on L that is within the rectum, and y_p is the most posterior point on L that is within the prostate. Variable x_o was chosen to be the center of the urethra as seen on the midaxial slice.

If G_{Dpr} and G_{Apr} refer to the gradients of radiation dose and chemical agent, respectively, then G_{pr} is defined as $G_{pr} = G_{Apr}/G_{Dpr}$

Therefore, G_{pr} is defined as the gradient of drug concentration in the prostate–rectum direction, relative to the radiation dose gradient.

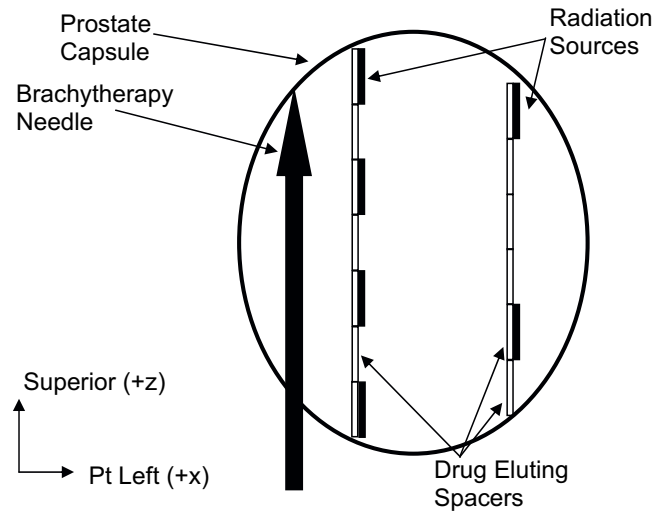


Fig. 2. Schematic drawing showing the coordinate system and the calculated location of chemically activated brachytherapy spacers (eluters). Eluters were considered to be at all possible eluter locations even though a source may also be there.

$G_{Apr} > 1$ implies that the gradient of the drug concentration (hence, sensitization) at a point is greater than the gradient of the radiation dose, *i.e.*, drug sources produce biologically sensitized regions that are more conformal than the radiation dose distribution alone. G_{pr} was evaluated for a number of points on the midsagittal plane and a series of values of z_0 between the superior extent and inferior extent of the prostate with a 0.25 cm spacing.

Radiosensitization-based treatment plan

We also modified the brachytherapy plan of 1 patient to illustrate the ability to locally enhance the effect of radiation by appropriate placement of drug-eluting spacers at a region that is at high risk for recurrence (as potentially identified via functional imaging). A region of interest (ROI) was identified, and a distribution of drug-eluting spacers was placed on a uniform 0.5-cm grid around that point while remaining at least 7 mm from a nearby normal structure (urethra). Radiosensitization enhancement factors of 1.2 to 1.8 for single-fraction doses of 2 to 10 Gy have been reported for taxol (18), and its radiosensitization efficiency depends on local drug concentration. Radiosensitizations of 1.6 to 5.8 were reported for cisplatin (both low- and high-dose rates) and 1.7 to 2.9 (19) for gemcitabine (pulsed low-dose-rate brachytherapy) (20). As a conservative approach to incorporate a typical anticipated radiosensitization enhancement in our calculations, we assumed the spacers to be loaded with a radiosensitizer that, in conjunction with low-dose-rate brachytherapy, provides a sensitization of 1.5 for concentrations of $A_0/10$ or higher. A linear decrease in radiosensitization from 1.5 to 1.0 for drug concentrations between $A_0/10$ and $A_0/50$, respectively, was assumed, and no radiosensitization was accounted for lower concentrations. Generation of drug around an eluter was assumed to be time invariant, *i.e.*, a steady-state three-dimensional drug distribution was assumed to be present in the tumor throughout radiation treatment. Thus, changes resulting from changes in the rate of drug diffusion from the eluter or changes in tumor biology (due to changes in vascularization) were not accounted for in the present approximation.

RESULTS

Lung SBRT sensitization

The curves in Fig. 1 suggest that for small values of ϕ_b , depths of drug penetration ~ 10 to 20 mm are obtained around each eluter while also retaining drug concentrations greater than the sensitization limit, $A_0/10$. Assuming four spherical eluters (radiopaque fiducials) placed within spherical lung tumors prior to SBRT, the calculations in Fig. 3a show that eluters of 0.5-mm radius provide sensitization to only a small portion of the tumor volume, unless ϕ_b is < 0.03 (*i.e.*, unless the drug has a long diffusion distance and is eliminated slowly from the area). Alternatively, four drug-loaded fiducials of 2-mm radius combined with ϕ_b of < 0.1 can provide 100% coverage of small tumors (Fig. 3b). Assuming that drug concentrations in excess of $A_0/10$ provide significant radiosensitization for radiation fraction sizes (12–20 Gy) employed in lung SBRT, ϕ_b of < 0.1 leads to the possibility of delivering reduced radiation to centrally located lung lesions for the same biological effect, thus leading to reduced normal tissue toxicity.

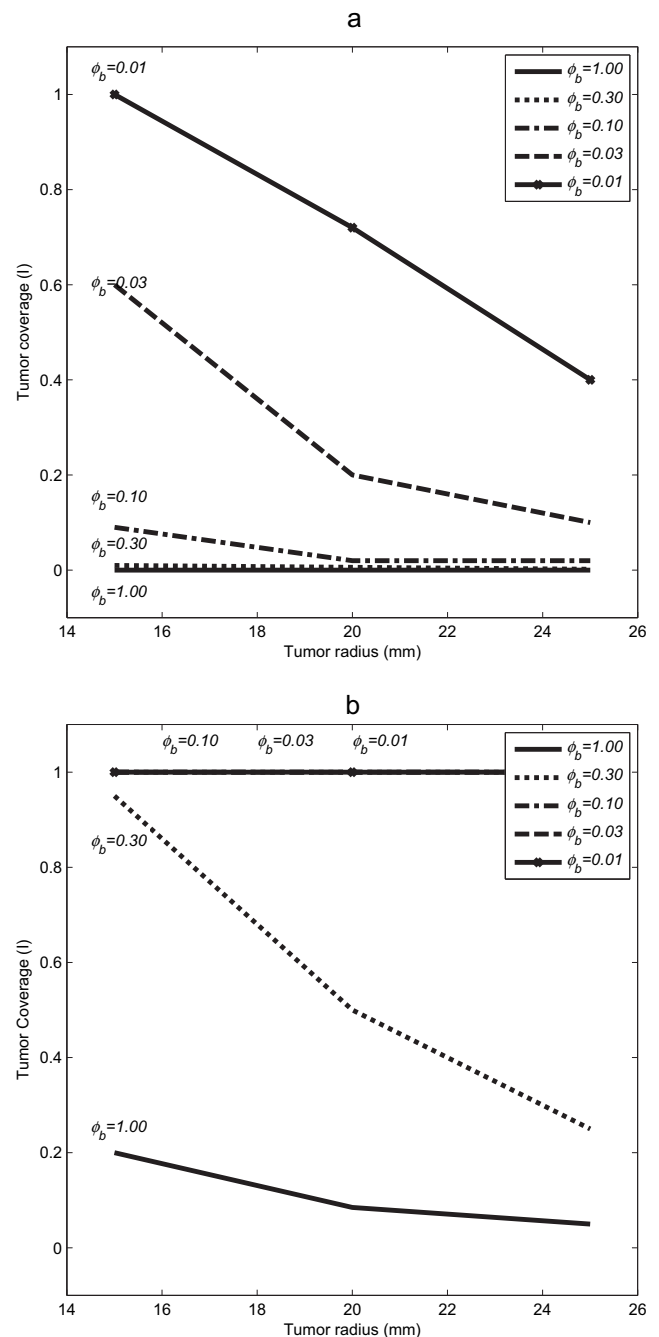


Fig. 3. Modeling of tumor coverage by radiosensitizer, assuming four regularly placed drug-loaded fiducials in small lung tumors, representing typical lung SBRT treatments. (a) Tumor coverage for small (radius = 0.5 mm) eluters. Large values of ϕ_b cannot sensitize a significant portion of the tumor, while low values of ϕ_b enable sensitization of 10% to 60% of small (<20-mm radius) tumors. (b) Tumor coverage for large (radius = 2 mm) eluters. Large eluters can sensitize most or all of the tumor for a variety of effective drug penetrations. For example, all values of ϕ_b would sensitize the entire tumor volume.

Brachytherapy sensitization: patient characteristics and source distributions

The brachytherapy preplans for 6 patients who received ^{125}I TRUS-guided permanent implants at our center were analyzed to calculate the drug distributions that would result by

Table 1. Patient and implant characteristics

Patient	Volume (cc)	No. of ^{125}I sources	No. of spacers
a	14	36	34
b	20	47	66
c	35	65	87
d	36	66	97
e	45	77	128
f	46	81	111

assuming that the spacers routinely placed between ^{125}I sources can optionally also become drug eluters and without modifying the planned implant process. A summary of implant characteristics for the six patients analyzed is shown in Table 1.

To provide flexibility in shaping the overall biological effect in the target volume, ideally, the drug concentrations should not be tightly correlated with radiation dose. In Fig. 4, the radiation dose and drug concentrations in the vicinity of the ^{125}I sources and eluters are compared for 1 patient assuming a ϕ_b of 0.08 mm^{-1} . There is a fraction of eluters that are very close (coincide) to the radioactive sources. However, the majority of eluters (high-drug-concentration positions) are not correlated with the position of the ^{125}I sources (high-radiation-dose positions). Hence drug-loaded spacers in brachytherapy procedures could deliver radiosensitizing drug (high-concentration points) to selected regions where the radiation dose from ^{125}I is low.

Constraints from metrics

While analysis of a small number of drug eluters (Fig. 3) calls for large eluter size and low values of ϕ_b to provide good target coverage, brachytherapy spacers often have small dimensions. Therefore, small-size eluters of 0.5-mm radius were modeled first. Figure 5a shows that an increased effective drug penetration in tissue ($\phi_b < 0.3$) is necessary to provide consistent biologically effective drug concentrations to substantial volume fractions (I_p) of the prostate gland for patient f. On the other hand, increasing the drug's penetration may also lead to drug diffusion beyond the prostate capsule, with subsequent sensitization of the rectum, which can reduce the therapeutic ratio. To enable drug distributions that are spatially more localized than radiation, the gradient of drug concentration relative to the radiation dose gradient, G_{pr} , must be greater than 1, which calls for ϕ_b of $>.05$ in Fig. 5a. Figure 5b shows the compounded results from the treatment geometries for all 6 patients examined. For these patients, who represent the range of gland sizes usually treated at our center, it can be seen that the window of opportunity for producing an improvement in the therapeutic ratio by using *in situ* release of radiosensitizer lies in the range $0.3 > \phi_b >.05$. Figure 5c shows an analysis similar to Fig. 5b, assuming placement of eluters of 2-mm radius within the prostate. For these larger eluters, it is the G_{pr} gradient constraint that is more significant than the effective drug diffusion, as substantial tumor coverage is achieved over the full range of ϕ_b analyzed. According to Fig. 5c, which shows results

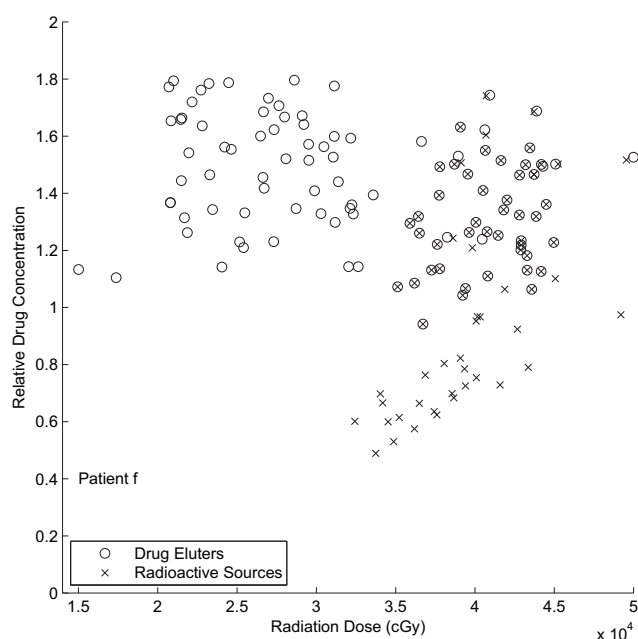


Fig. 4. A scatter plot showing radiosensitizer concentration and radiation dose in the vicinity of drug-eluting spacers and radiation sources, respectively, for patient f. Circles represent drug concentration values sampled at the location of the eluters, while crosses represent radiation dose values sampled at the location of ^{125}I sources. Due to the decoupling of drug and radiation sources, a new degree of freedom to optimize the biological effect is created.

from all 6 patients together, values of $\phi_b > 0.25$ would provide drug concentration gradient profiles that are more localized than the radiation dose distributions ($G_{pr} > 1$). Given that experimentally inferred 11 values of ϕ_b for paclitaxel in the monkey brain lie in the range of 0.4 to 1.3 mm^{-1} , arranging eluters to fulfill the constraints suggested by Fig. 5c may be technically feasible.

Eluter planning for BIS-IGRT dose painting

Using eluters to enhance the effect of ^{125}I seeds creates the additional possibility of incorporating optimal eluter configurations in treatment planning and adjusting needle placement to accommodate the overall biological (radiation-plus-drug) effect. Accordingly, subvolume biological enhancements can be achieved to boost high-risk tumor regions revealed, for example, via magnetic resonance spectroscopy or positron emission tomography. To this end, a brachytherapy plan was used to demonstrate localized delivery of a drug to a hypothetical ROI within the prostate while sparing the nearby urethra and the rectum. The resulting combined brachytherapy plan (Fig. 6d) meets the clinical planning criteria routinely applied at our center while also boosting biological dose to the ROI without the use of additional ^{125}I radiation sources. If one achieved an equivalent ROI boost using additional ^{125}I brachytherapy sources within the ROI, this would deliver 30% and 60% additional dose to the rectum and urethra, respectively (calculation not shown). In contrast, the localized drug distribution using BIS-IGRT delivers less biological dose to the normal structures than is achievable using radiation dose painting alone.



Fig. 5. Modeling of tumor coverage by radiosensitizer, assuming implantation of drug-loaded spacers for the geometry of 6 patients treated with prostate TRUS-guided ^{125}I brachytherapy. The two treatment planning metrics of interest, I_p (tumor coverage, open circles, O) and G_{pr} (drug concentration gradient relative to radiation dose gradient, crosses, X) are plotted as a function of ϕ_b . For any given ϕ_b , the values for G_{pr} are calculated at several different points on the midsagittal plane. (a) Analysis for the anatomy and eluter configuration in the prostate treatment of patient f for eluters of 0.5-mm radius. Values of ϕ_b progressively less than 0.3 result in substantial (>20%) tumor coverage. On the other hand, values of ϕ_b progressively higher than 0.06 result in G_{pr} of >1. A G_{pr} value greater than 1 indicates drug distributions with a gradient that is steeper than the radiation dose gradient and a “tight” modulation of radiosensitization. (b) Analysis for the anatomy and eluter configuration of all 6 patients bunched together in a single graph for eluters of 0.5-mm radius. The window of opportunity between the two competing constraints on ϕ_b (prostate coverage I_p versus drug concentration gradient G_{pr}) is demonstrated. (c) Analysis for the anatomy and sources configuration of all 6 patients bunched together in a single graph for eluters of 2-mm radius. For these larger eluters, all values of $\phi_b > 0.25$ would provide drug concentration gradient profiles that are more localized than the radiation dose distributions, G_{pr} of >1. Some of the existing formulations of taxol-based radiosensitizers (paclitaxel, taxotere) have experimentally inferred ϕ_b values in the range of 0.4 to 1.3 mm^{-1} in tissue (26).

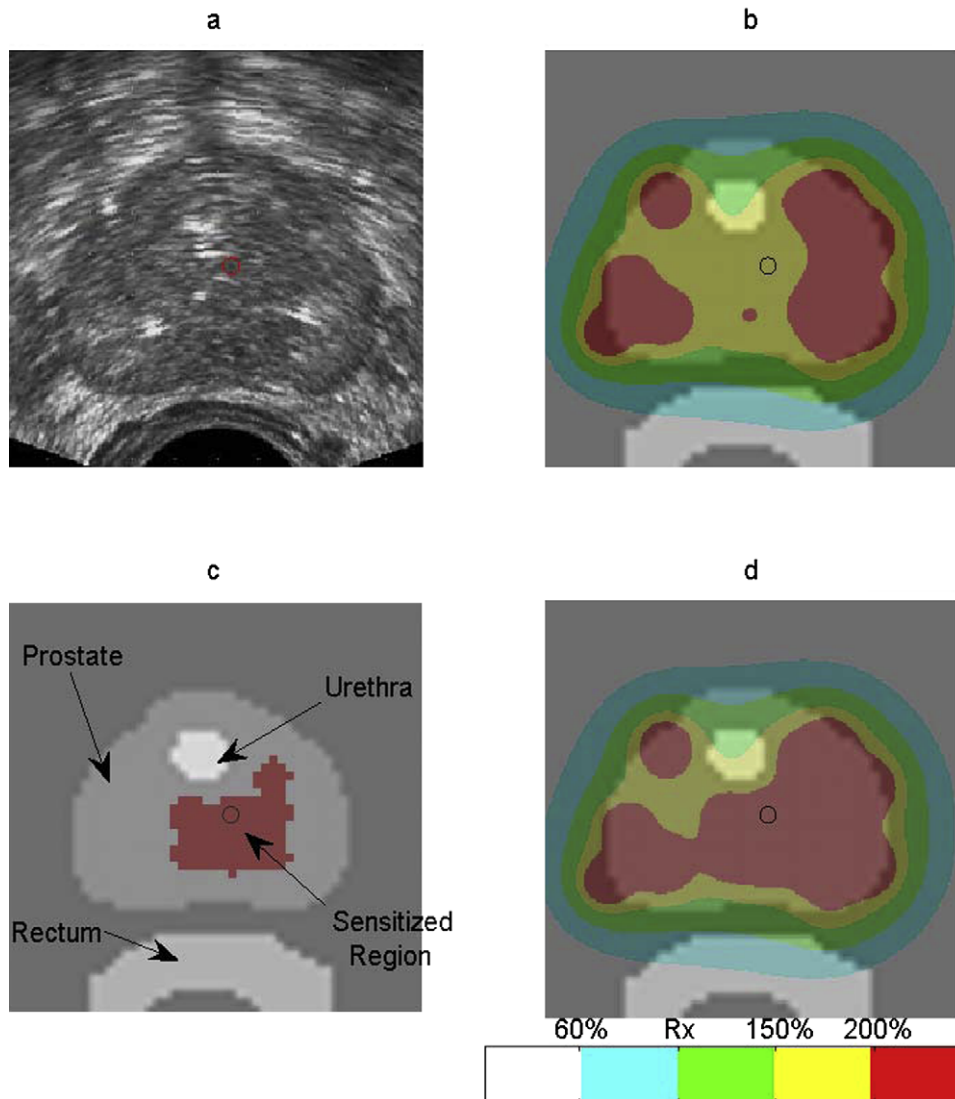


Fig. 6. Effect of BIS-IGRT for prostate brachytherapy on patient f. (a) Patient anatomy (patient f) as visualized in a TRUS-guided ^{125}I brachytherapy procedure. A hypothetical high-risk radio-resistant tumor ROI is indicated by a small circle (O). (b) Color wash indicating radiation-only dose distribution planned for this brachytherapy case. Green and yellow represent regions of dose greater than the prescription dose and less than 150% of prescription; blue is less than the prescription; and red is 200% of prescribed dose. Dose was calculated on a Nucletron SPOT system (Nucletron B.V., Veenendaal, Netherlands) using computer optimization followed by manual adjustments. (c) Drug-only distribution of radiosensitizer released from deliberately implanted drug-eluting spacers activated around the high-risk ROI. (d) Combined biologically effective dose resulting from ^{125}I radiation plus the anticipated radiosensitization of the subvolume where radiosensitizer is present. Boosting of the radio-resistant region is achieved without significantly increasing biologically effective doses to the rectum or the urethra.

DISCUSSION

Intravenous administration of biologically active drugs for cancer treatment (taxotere, 5-fluorouracil, adriamycin, and others) together with radiation is commonly used for cancer treatment but is ultimately limited by systemic toxicity. Methods for *in situ* drug delivery to tumors, which can result in significantly lower systemic toxicity while also enabling higher drug doses to the tumor (12) have also been reported. These methods include intratumoral implantation of cytotoxic drug-loaded crystals (21), slow-release polymers (8, 9, 12, 22), liposomes (13), microspheres (14), and nanospheres (23). However, due in part to the invasiveness of *in*

situ placement procedures, few clinical trials attempting to implement this approach have been reported (22). Modern radiation therapy practice routinely implants markers in tumors and thus provides an opportunity for improving the therapeutic ratio using *in situ* drug delivery systems without additional invasive procedures than are already used. We therefore adapted drug delivery calculations previously reported for single-drug slow-release polymers (12, 13) to fit the multifiducial/multispacer configurations used in modern treatments such as lung SBRT or prostate brachytherapy, in conjunction with real patient geometries. Using hypothetical drug-loaded IGRT fiducials and brachytherapy spacers as eluters of

biologically active reagents, we provide a first approximation to three-dimensional biologically equivalent treatment planning that accounts for the spatial distributions of radiosensitizer sources within the planning treatment volume.

Our calculations highlight the suitability of ϕ_b , the diffusion–elimination modulus, as a parameter to describe phenomenologically drug concentrations versus distance from the source. Lower ϕ_b values lead to larger effective diffusion and are desirable for improved target coverage, while higher ϕ_b values produce drug distributions that are more localized than brachytherapy radiation treatments. ϕ_b values that provide radiosensitization of tumor subvolumes without significant sensitization of neighboring structures define windows of opportunity between the competing constraints. Depending on the particular treatment site and situation, ϕ_b for a particular drug-eluter combination can be selected to fit the existing constraints. The availability of several chemical forms or carriers of the same active compound in conjunction with multiple slow-release formulations provides substantial flexibility in this respect. Experimental study of time-release and total drug capacity properties of tissue-implanted devices (in preclinical models) are required in future studies to derive ϕ_b values for specific drug formulations and to enable three-dimensional calculations of drug distributions. Specific drug formulations will also have to account for additional biological dependencies, such as variability of diffusion depending on tissue/tumor type, tumor vascularity, degree of fibrosis, dependence of radiosensitization on dose rate and fraction

size, and other variables (7). The results of these efforts could converge to a treatment planning system that would shape and optimize biological effect by means of simultaneous computation of radiation dose and drug distributions.

CONCLUSIONS

The potential for BIS-IGRT illustrated herein also encompasses the possibility of matching locally delivered biologically active compounds to the individual tumor biology as defined via molecular tumor profiling (biological imaging [24] or molecular DNA/RNA analysis of the primary tumor [25]). For example, a tumor demonstrating increased angiogenesis via imaging (26) could be considered for therapy augmentation via locally placed angiogenesis inhibitors (anti-VEGF drug-loaded fiducials), and a prostate tumor revealed to be BRCA1/2 negative via molecular analysis could be implanted with poly-ADP-ribose-polymerase inhibitor loaded spacers (27) prior to brachytherapy to provide optimal three-dimensional biologically equivalent therapy. The combination of highly specific *in situ*-administered molecularly targeted agents with a relatively nondiscriminatory agent such as radiation may provide improved approaches for local tumor control. The combination of BIS-IGRT, molecular tumor profiling, and nanofabrication of slow-release devices contains synergies that can be exploited for personalized cancer radiation treatment.

REFERENCES

1. Timmerman R, McGarry R, Yiannoutsos C, *et al.* Excessive toxicity when treating central tumors in a phase II study of stereotactic body radiation therapy for medically inoperable early-stage lung cancer. *J Clin Oncol* 2006;24:4833–4839.
2. Cormack RA, Kooy H, Tempany CM, *et al.* A clinical method for real-time dosimetric guidance of transperineal ^{125}I prostate implants using interventional magnetic resonance imaging. *Int J Radiat Oncol Biol Phys* 2000;46:207–214.
3. Kaplan ID, Meskell P, Oldenburg NE, *et al.* Real-time computed tomography dosimetry during ultrasound-guided brachytherapy for prostate cancer. *Brachytherapy* 2006;5:147–151.
4. Wurm RE, Gum F, Erbel S, *et al.* Image guided respiratory gated hypofractionated Stereotactic Body Radiation Therapy (H-SBRT) for liver and lung tumors: Initial experience. *Acta Oncol* 2006;45:881–889.
5. Gultepe E, Nagesha D, Menon L, *et al.* High-throughput assembly of nanoelements in nanoporous alumina templates. *Appl Phys Lett* 2007;90:163119.
6. Garcia-Garcia HM, Vaina S, Tsuchida K, *et al.* Drug-eluting stents. *Arch Cardiol Mex* 2006;76:297–319.
7. Yang C, Burt HM. Drug-eluting stents: Factors governing local pharmacokinetics. *Adv Drug Deliv Rev* 2006;58:402–411.
8. Li Y, Owusu A, Lehnert S. Treatment of intracranial rat glioma model with implant of radiosensitizer and biomodulator drug combined with external beam radiotherapy. *Int J Radiat Oncol Biol Phys* 2004;58:519–527.
9. Doiron A, Yapp DT, Olivares M, *et al.* Tumor radiosensitization by sustained intratumoral release of bromodeoxyuridine. *Cancer Res* 1999;59:3677–3681.
10. Crank J. *The Mathematics of Diffusion*, 2nd edition. New York: Oxford University Press; 1979.
11. Mak M, Fung L, Strasser JF, *et al.* Distribution of drugs following controlled delivery to the brain interstitium. *J Neurooncol* 1995;26:91–102.
12. Fung LK, Ewend MG, Sills A, *et al.* Pharmacokinetics of interstitial delivery of carmustine, 4-hydroperoxycyclophosphamide, and paclitaxel from a biodegradable polymer implant in the monkey brain. *Cancer Res* 1998;58:672–684.
13. Chen D, Song D, Wientjes MG, *et al.* Effect of dimethyl sulfoxide on bladder tissue penetration of intravesical paclitaxel. *Clin Cancer Res* 2003;9:363–369.
14. Li KW, Dang W, Tyler BM, *et al.* Polylactofate microspheres for Paclitaxel delivery to central nervous system malignancies. *Clin Cancer Res* 2003;9:3441–3447.
15. Maeda H, Wu J, Sawa T, *et al.* Tumor vascular permeability and the EPR effect in macromolecular therapeutics: A review. *J Control Release* 2000;65:271–284.
16. Tada H, Higuchi H, Wanatabe TM, *et al.* In vivo real-time tracking of single quantum dots conjugated with monoclonal anti-HER2 antibody in tumors of mice. *Cancer Res* 2007;67:1138–1144.
17. Kong G, Braun RD, Dewhirst MW. Hyperthermia enables tumor-specific nanoparticle delivery: Effect of particle size. *Cancer Res* 2000;60:4440–4445.
18. Tishler RB, Geard CR, Hall EJ, *et al.* Taxol sensitizes human astrocytoma cells to radiation. *Cancer Res* 1992;52:3495–3497.
19. Raaphorst GP, Wang G, Stewart D, *et al.* Concomitant low dose-rate irradiation and cisplatin treatment in ovarian

- carcinoma cell lines sensitive and resistant to cisplatin treatment. *Int J Radiat Biol* 1996;69:623–631.
20. Castro Kreder N, Van Bree C, Franken NA, *et al.* Effects of gemcitabine on cell survival and chromosome aberrations after pulsed low dose-rate irradiation. *J Radiat Res (Tokyo)* 2004;45: 111–118.
 21. von Eckardstein KL, Patt S, Kratzel C, *et al.* Local chemotherapy of F98 rat glioblastoma with paclitaxel and carboplatin embedded in liquid crystalline cubic phases. *J Neurooncol* 2005; 72:209–215.
 22. Vukelja SJ, Anthony SP, Arseneau JC, *et al.* Phase 1 study of escalating-dose OncoGel (ReGel/paclitaxel) depot injection, a controlled-release formulation of paclitaxel, for local management of superficial solid tumor lesions. *Anticancer Drugs* 2007; 18:283–289.
 23. Jabr-Milane L, van Vlerken L, Devalapally H, *et al.* Multi-functional nanocarriers for targeted delivery of drugs and genes. *J Control Release* 2008;130:121–128.
 24. Ling CC, Humm J, Larson S, *et al.* Towards multidimensional radiotherapy (MD-CRT): Biological imaging and biological conformality. *Int J Radiat Oncol Biol Phys* 2000;47:551–560.
 25. Li J, Wang L, Mamon H, *et al.* Replacing PCR with COLD-PCR enriches variant DNA sequences and redefines the sensitivity of genetic testing. *Nat Med* 2008;14:579–584.
 26. Cai W, Chen K, Mohamedali KA, *et al.* PET of vascular endothelial growth factor receptor expression. *J Nucl Med* 2006;47: 2048–2056.
 27. Farmer H, McCabe N, Lord CJ, *et al.* Targeting the DNA repair defect in BRCA mutant cells as a therapeutic strategy. *Nature* 2005;434:917–921.